Soft Matter

Cite this: *Soft Matter*, 2012, **8**, 8294

www.rsc.org/softmatter

COMMUNICATION

Insertion mechanism of cell-penetrating peptides into supported phospholipid membranes revealed by X-ray and neutron reflection†

D. Choi,[a] J. H. Moon,[b] H. Kim,[a] B. J. Sung,[a] M. W. Kim,[b] G. Y. Tae,[c] S. K. Satija,[d] B. Akgun,[de] C.-J. Yu,[f] H. W. Lee,[f] D. R. Lee,[g] J. M. Henderson,[h] J. W. Kwong,[h] K. L. Lam,[h] K. Y. C. Lee*[h] and K. Shin*[a]

Received 19th April 2012, Accepted 12th June 2012
DOI: 10.1039/c2sm25913c

X-Ray and neutron reflectivity measurements on systems composed of a 1,2-dipalmitoyl-*sn*-glycero-3-phosphocholine (DPPC) bilayer and transcription-activating-factor derived peptides (TDPs) have allowed us to determine the mechanism of membrane translocation. By monitoring the structural changes of the bilayers caused by the binding of TDPs while systemically varying temperature and TDP concentration, our results revealed the detailed molecular structures of the stepwise interactions that occurred during the translocation of TDP across the lipid bilayers. While little indication of membrane perturbation was observed at low TDP concentrations, we found that the TDP movement across the membrane induced defect formations in the membrane at higher TDP concentrations.

Cell-penetrating peptides (CPPs) are short peptides that can traverse cell membranes efficiently[1,2] with an attached moiety and are effective for a variety of target cells.[3,4] Among CPPs, the transcription-activating-factor (TAT)-derived peptide (TDP) from the human-immunodeficiency-virus (HIV-1) TAT protein is the most widely studied.[5,6] Extensive cell-based experiments have shown that membrane translocation of TDP is energy-independent and non-receptor mediated,[7,8] but the molecular mechanism is not clear. As an alternative, the use of a model lipid system may provide a suitable platform for elucidating the underlying mechanism for the translocation by eliminating many variables associated with the complexity of the cell membrane. Previously, the adsorption of TDP onto a lipid monolayer composed of 1-palmitoyl-2-oleoyl-*sn*-glycero-3-phospho-*rac*-glycerol and 1-palmitoyl-2-oleoyl-*sn*-glycero-3-phosphocholine has been characterized; however, no peptide insertion into the lipid monolayer was observed at the bilayer equivalent pressure. It has therefore been thought that direct penetration of TDP into a lipid membrane is not possible.[9]

In contrast, a plausible mechanism, which consists of four steps, has recently been suggested based on molecular dynamics (MD) simulations for the spontaneous translocation of TDP across lipid membranes.[10] According to this mechanism, TDP binds to the membrane surface due to an attractive electrostatic interaction with the phosphate lipid head group. The increase in peptide concentration leads to a significant local deformation of the membrane structure, which permits the translocation of arginine side chains of the peptide from the outer to the inner leaflet of the membrane, and becomes a seed for pore formation. Once a pore is formed, other peptides can translocate in an energy-independent manner with a lifetime of the order of microseconds, rendering the translocation process difficult to observe in experiments.

Here, we provide for the first time experimental evidence for the energy-independent translocation of TDP and TDP-induced defects in the membrane. We have obtained clear X-ray reflectivity (XR) evidence for the penetration of TDP into lipid bilayers composed exclusively of zwitterionic 1,2-dipalmitoyl-*sn*-glycero-3-phosphocholine (DPPC), leading us to conclude that cell membrane translocation of TDP results from its intrinsic ability to move across a lipid bilayer without the aid of any other cell surface molecules. Neutron reflectivity (NR) and atomic force microscopy (AFM) measurements further reveal the creation of defects as a result of the translocation.

NR measurements were performed at the National Institute of Standards and Technology (Gaithersburg, MD) using the NG7 horizontal reflectometer ($\lambda = 4.75$ Å). The beam size is horizontally 35 mm, and the vertical width was varied to maintain a constant footprint on the sample. XR measurements were performed at Pohang Accelerator Laboratory, Korea (wiggler beamline 5A). At the sample position, the focused beam size was 500 μm (H) × 400 μm (V). X-Ray photons entered and exited the liquid cell through Kapton windows, and the 20 keV X-ray beam could transmit directly into liquid medium with ~50% absorption.[11,12] The samples for the XR and the NR measurements were prepared on Si wafers (10 mm × 10 mm) and Si slabs (diameter = 76 mm), respectively. NR and XR data were collected at the solid–liquid interface up to $Q_{z,\max} \approx 0.22$ Å^{-1} and 0.35 Å^{-1}, respectively. For the preparation of supported

[a]*Department of Chemistry, Institute of Biological Interfaces, Sogang University, Seoul 121-742, Korea. E-mail: kwshin@sogang.ac.kr; Tel: +82 2 705 8441*
[b]*Department of Physics, KAIST, Daejon 305-741, Korea*
[c]*Department of Materials Science and Engineering, GIST, Gwangju 500-712, Korea*
[d]*NIST Center for Neutron Research, Gaithersburg, MD 20899-6100, USA*
[e]*Department of Materials Science and Engineering, University of Maryland, College Park, MD 20742, USA*
[f]*Pohang Accelerator Laboratory, POSTECH, Pohang 790-784, Korea*
[g]*Department of Physics, Soongsil University, Seoul 156-743, Korea*
[h]*Department of Chemistry, Institute for Biophysical Dynamics and James Franck Institute, University of Chicago, Chicago, IL 60637, USA. E-mail: kayeelee@uchicago.edu*
† Electronic supplementary information (ESI) available: See DOI: 10.1039/c2sm25913c

lipid bilayers on Si substrate, the fusion method of small unilamellar vesicles was used, and the resulting bilayer covers 88% of the substrate (Fig. S1†).

Fig. 1 shows the XR curves measured from a supported lipid bilayer (SLB; solid circles) and fitted using the *Parratt* formula modified for rough interfaces (black line). The footprint correction has been applied when fitting the raw data. To check the sensitivity of the XR curves to the structure of TDP on/in the lipid bilayer, we simulated two specific cases: (1) adsorption of TDP onto the top of the outer leaflet and (2) insertion of TDPs into the lipid bilayer and accumulation near the inner head group, each giving rise to a thickening by 6 Å in the respective headgroup region (Fig. 1b). For TDP adsorption, only an increase in the distal layer with a small density contrast is incorporated in the simulated profile; this manifests itself as a decrease in the dip-to-dip distance of the thickness fringes and a shift in the dip positions to lower values (red dashed line in Fig. 1). On the other hand, the situation of TDP insertion is given by an increase in the layer thickness of the inner leaflet, and the associated headgroup region shows a noticeable change in its density profile; a significant shift in the position of the first dip of the fringes in the XR curves can be easily discerned (green dashed lines in Fig. 1).

Armed with these simulation results, we proceeded to use XR to monitor structural changes in a supported DPPC bilayer with TDP present. The displaced curves in Fig. 2a correspond to the same supported DPPC bilayer during the injection and incubation processes: (1) the initial structure of SLB formed *via* a vesicle fusion process at 25 °C, (2) the SLB with a 1 μM TDP medium at 25 °C, (3) the SLB of (2) after incubation at 55 °C for 4 h and cooling to 25 °C, (4) the SLB after the injection of additional TDP stock solution to result in a final 11 μM TDP medium at 25 °C and (5) the SLB of (4) after incubation at 55 °C for 2 h and cooling to 25 °C. As TDP is a short peptide without any well-defined secondary structure, the temperature cycling should not have any effect on the peptide structure. We have also demonstrated that temperature cycling does not result in additional loss of bilayer materials (see ESI, Fig. S2†). Each data set in Fig. 2a shows a unique set of interference fringes, containing only the form factor for the system without a Q_z^{-4} decay. The solid lines in Fig. 2a are fits to the data (symbols) obtained using the corresponding dispersion profiles (colored lines) shown in Fig. 2b. The dispersion δ is linearly related to the electron density ρ, given by $\delta = \lambda^2 \rho r_o / 2\pi$, where r_o is the classical electron radius.

First, we discuss the layered structures of the SLB before and after TDP injection for the 1 μM system at 25 °C, a temperature below the

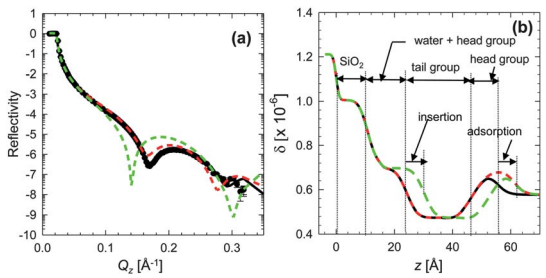

Fig. 1 (a) XR curve of a DPPC bilayer (closed circles). The black line is the best fit. Red and green dashed lines are fits to the data using adsorption and insertion models. (b) Their corresponding total dispersion profiles. For the simulation of TDP adsorption onto the head groups of the outer (red dashed line) and the inner (green dashed line) leaflets, the respective headgroup regions were thickened by 6 Å.

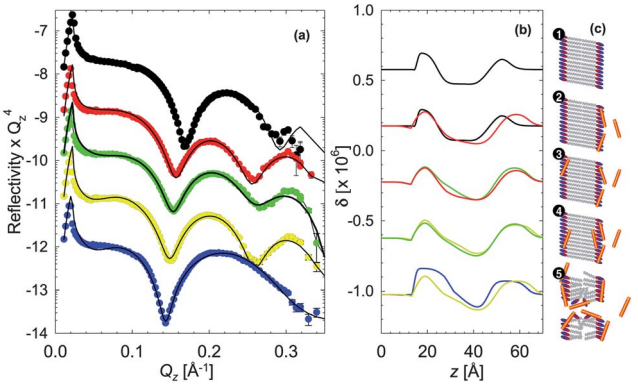

Fig. 2 (a) XR curves for a DPPC bilayer (1) before and (2) after adding 1 μM of TDP solution at 25 °C, (3) after incubating at 55 °C, (4) after increasing TDP to 11 μM of TDP solution at 25 °C, and (5) after incubating at 55 °C. Solid lines represent model fits to the experimental data corresponding to the dispersion profiles (colored lines) in (b), where 2 profiles are shown in (2)–(5) for direct comparison with the previous case. (c) SLB models are schematically represented: (1) a pristine SLB, (2) TDP adsorption onto an outer leaflet, (3) insertion into an inner leaflet, (4) further adsorption of TDP onto an outer leaflet, and (5) formation of pores across SLB.

gel–fluid transition temperature of DPPC, $T_{lc} \approx 42$ °C (Fig. 2a(1) and (2)). The XR curve in Fig. 2a(1) shows well-defined Kiessig fringes; two distinct regions from the inner and the outer head groups are separated by the corresponding tail regions. After the introduction of 1 μM TDP medium, the period of Kiessig fringes in Fig. 2a(2) decreases significantly, indicating an increased distance between the centers of the headgroup regions of the inner and outer leaflets. Results from fits using the 5-layered model confirm thickening of the sample. While the thickness of the tail region remains unchanged, the outer headgroup region is thickened by 6 Å, indicating that the injected TDPs were predominantly adsorbed onto the outer leaflet at this temperature. Further incubation at 55 °C did not significantly affect the thickness of the film as shown in Fig. 2b(3).

When the TDP-buffer medium concentration for the same SLB was increased to 11 μM at 25 °C, the reflectivity curve still remained rather similar to that for the 1 μM solution (Fig. 2a(4)), indicating that the adsorbed TDP at the outer leaflet was already quite saturated even at 1 μM. At 25 °C, the DPPC bilayer is in the gel phase; we believe that the tail region is tightly packed and presents itself as a rigid barrier, resisting the penetration of TDP molecules. Lipid molecules in the gel phase are thought to be unable to diffuse laterally, so penetration of TDPs could be very difficult at $T < T_{lc}$. However, after incubating the SLB with this increased TDP concentration at 55 °C, which is above T_{lc}, and re-measuring XR after cooling the sample back to 25 °C, the observed oscillation became much broader, indicating that the distance between the two headgroup regions had decreased significantly. This membrane thinning effect is clearly observed in the dispersion profile obtained from the fit (see Fig. 2b(5)). The increase in electron density near the inner head group and the tail group is indicative of the transfer of the TDP (which has the highest electron density among participating components) from the outer to the inner leaflet during the heating process at $T > T_{lc}$, and its subsequent accumulation inside the bilayer.

These observations based on our X-ray data are very much in line with the recently reported MD simulation data in ref. 10; TDP

accumulates on the outer leaflet and then penetrates into the inner leaflet of a fluid membrane *via* a membrane thinning process facilitated by the electrostatic interaction between the positively charged TDP and the negatively charged phosphate group of the inner leaflet. The mass transfer of TDP is predicted to be accelerated when the highly saturated TDP on the outer leaflet forms pores. Though X-ray results indicate that the highly charged TDP molecules accumulate at the headgroup regions on both the distal and proximal leaflets, the mechanism by which the peptide reaches the proximal leaflet and the presence of pore-like structures cannot yet be verified with the experimental techniques described above, owing to the insensitivity of XR to in-plane structures and the small difference in electron density between water and lipid tails.

To obtain this information, we have turned to NR which makes contrast enhancement possible *via* deuteration. A series of schematic models and their corresponding scattering length density (SLD) profiles are shown in Fig. S3a† when defects form across a SLB. Since NR detects variations of the SLD in the direction normal to the surface, z, a fully occupied SLB immersed in a D_2O-based buffer solution provides the highest contrast. As shown in Fig. S3a(1)†, a SLD profile consists of Si/SiO_2, an inner D_2O cushion layer, a SLB, and an outer D_2O medium. If pore-like structures are formed across the SLB due to the presence of TDP, they will be filled with D_2O, and consequently, the averaged SLD of the SLB region will be increased. Since the SLB has the lowest SLD, increase in SLD should be linearly proportional to the total lipid-absent volume filled with D_2O. In order to test whether the SLD variation due to defect formation at the membrane interface can change the reflectivity spectrum significantly, we further simulated NR curves as we varied the SLD of the SLB systemically (Fig. S3b†). As the occupied volume of defects was increased, the positions of the first two minima at 0.04 and 0.15 $Å^{-2}$ remained roughly the same. However, the intensity of the first minimum decreased, indicating that the NR profile is indeed sensitive to D_2O occupying the lipid-absent space in the membrane.

Fig. 3a shows the NR data (symbols) and the corresponding fits (lines) obtained at 25 °C after incubation at 55 °C for $C = 0$, 1.2, 2.4, and 4.8 μM TDP solutions. The overall trend due to TDP injection is very similar to that from simulation results (see Fig. S2b†). Closer examination of the simulated and experimental NR profiles reveals some differences in their fine features, likely due to the fact that details of the SLB are omitted in the simulated version. The corresponding fitting models are shown in Fig. 3b. The reflectivity profile shows a significant contrast between the supported bilayer and the D_2O buffer. The total bilayer thickness was found to be 56 ± 1 Å, in good agreement with the thickness from X-ray data. Initially a well-defined DPPC bilayer was measured in the D_2O-based buffer before any TDP injection, as shown in Fig. S2b.† The SLD of the tail region was somewhat higher than that for the ideal hydrocarbon chain; analysis shows that 12% of the surface is not covered by a bilayer, and the enhanced SLD in the SLB is due to the intervening D_2O. Interestingly, a negligible difference was observed between the curves before and after peptide injection for the 1.2 μM TDP solution. This finding is in agreement with our XR results with TDP at $C = 1.0$ μM (see Fig. 2b(3)), confirming that the presence of a low concentration of TDP does not lead to TDP translocation. Therefore, we can conclude that defect formation in the membrane is related to TDP penetration and that a concentration of ~1.0 μM is not enough to induce any detachment of lipid materials. However, when the TDP concentration was increased to 2.4 μM, the first minimum of the measured curve (Fig. 3a, open triangles) dropped significantly. We obtained a defect volume of about 24%, with a further increase to 30% at $C =$ 4.8 μM (see Fig. 4d). NR results at various concentrations of TDP pinpoint the threshold concentration for defect formation to be between 1.2 and 2.4 μM. The overall defect volume increased somewhat as the concentration was increased above the threshold value.

Note that CPPs *in vivo* have evolved to traverse cell membranes without causing irreversible damage since their function is to deliver cargo to target cells;[7] therefore, if long-lived pore structures were formed, the cell would perish from depolarization of the membrane potential, defeating the whole purpose of cargo delivery. It is, however, reasonable to assume that as CPPs traverse membranes from one leaflet to the other, they could in principle generate membrane curvature in a toroidal fashion in which the two leaflets are curved into each other. This would facilitate the passive transport of TDPs from the exterior to the interior of a cell, as observed *in silico*.[10] The increased SLD of D_2O within the membrane slab can be then explained by two possibilities: (1) the formation of pores stabilized by an integral number of peptides along the rim and (2) the creation of permanent membrane defects as a result of lipid removal.

AFM images in Fig. 4a–c clearly differentiate between these two scenarios, confirming that indeed the presence of TDP solubilizes the supported lipid bilayers removing the lipid material. As confirmed by

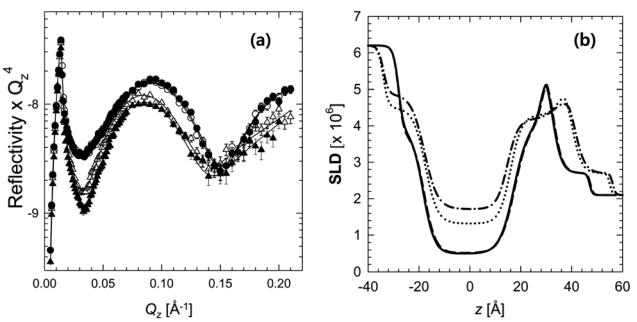

Fig. 3 (a) NR data (symbols) and corresponding fits (lines) at 25 °C after incubation at 55 °C: before (closed circles) and after injections of $C = 1.2$ μM (open circles), 2.4 μM (open triangles), and 4.8 μM (closed triangles) TDP solutions. (b) Corresponding SLD profiles of the curves shown in (a). The SLD profiles before injection (line) and after injection of $C = 1.2$ μM (dashes) are nearly superimposed. However, the SLDs in the region of lipid bilayer increase progressively after injection of $C = 2.4$ μM (dots) and 4.8 μM (dash-dots).

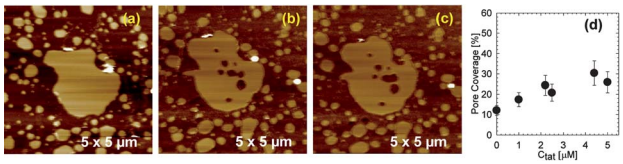

Fig. 4 AFM images of mica supported DMPC bilayers at 30 °C, which is above T_{lc}. (a) Before and (b) after injection TDP, and (c) scanned image of (b) after 18 min. (d) Calculated defect coverage obtained by NR *vs.* injected TDP concentrations. The lipid used in the AFM study was 1,2-dimyristoyl-*sn*-glycero-3-phosphocholine (DMPC), which has a lower T_{lc} (~23 °C).

XR, the TDPs distribute themselves across the two leaflets of the supported membranes. In principle, this could cause a rise in the local concentration of the peptide in association with the membrane to such an extent that solubilization might occur. This is seen in Fig. 4b, as both defects arise in the central large patch. Additionally patches surrounding the large central one are even removed. If pores did form, these structures would have been observed in all the patches both large and small. Hence we can conclude that the locations with lipids absent thus resemble more like surface defects than the pores in the biological sense.

Acknowledgements

This research was supported by the Mid-career Researcher Program (2011-0017539), the Global Frontier Research Program (2011-0032155), the PET Converging Research Center, Advanced Research Center for Nuclear Excellence, and a GIST-NCRC grant (R15-2008-006) funded by MEST, Korea.

References

1 M. Zorko and U. Langel, *Adv. Drug Delivery Rev.*, 2005, **57**, 529–545.
2 M. Lindgren, M. Hällbrink, A. Prochiantz and U. Langel, *Trends Pharmacol. Sci.*, 2000, **21**, 99–103.
3 H. Brooks, B. Lebleu and E. Vivès, *Adv. Drug Delivery Rev.*, 2005, **57**, 559–577.
4 B. Albarran, R. To and P. S. Stayton, *Protein Eng., Des. Sel.*, 2005, **18**, 147–152.
5 A. D. Frankel and C. O. Pabo, *Cell*, 1988, **55**, 1189–1193.
6 M. Green and P. M. Loewenstein, *Cell*, 1988, **55**, 1179–1188.
7 E. Vivès, P. Brodin and B. Lebleu, *J. Biol. Chem.*, 1997, **272**, 16010–16017.
8 D. Derossi, A. Joliot, G. Chassaing and A. Prochiantz, *J. Biol. Chem.*, 1994, **269**, 10444–10450.
9 A. Ziegler, X. L. Blatter, A. Seelig and J. Seelig, *Biochemistry*, 2003, **42**, 9185–9194.
10 H. D. Herce and A. E. Garcia, *Proc. Natl. Acad. Sci. U. S. A.*, 2007, **104**, 20805–20810.
11 C. E. Miller, J. Majewski, E. B. Watkins, D. J. Mulder, T. Gog and T. L. Kuhl, *Phys. Rev. Lett.*, 2008, **100**, 058103.
12 C. E. Miller, J. Majewski, T. Gog and T. L. Kuhl, *Phys. Rev. Lett.*, 2005, **94**, 238104.